Oxid Met (2017) 88:583–598
DOI 10.1007/s11085-017-9741-5

ORIGINAL PAPER

Effects of Ga, Sn Addition and Microstructure on Oxidation Behavior of Near-α Ti Alloy

Y. Yang[1,2] · T. Kitashima[1,2] · T. Hara[2] · Y. Hara[2] · Y. Yamabe-Mitarai[2] · M. Hagiwara[2] · S. Iwasaki[2]

Received: 28 November 2016 / Published online: 31 January 2017

Abstract We investigated the effects of adding Ga or Sn, with almost the same Al equivalent, on the oxidation behaviors of near-α Ti alloy with the bimodal structure and lamellar structure. The replacement of Sn with Ga decreased the alloy weight gain during oxidation, suppressed oxide growth, and improved adherence between the oxide and substrate. A lamellar alloy structure showed a lower weight gain during oxidation compared to the bimodal structure. Unlike conventional near-α alloys, recrystallization occurred near the oxide/substrate interface in Ga-modified alloy, which may contribute to the release of stress, improvement of the adherence between the oxide and substrate, and prevention of oxide-scale spallation from the Ga-modified alloy. A possible mechanism for the recrystallization in the Ga-modified alloy was also discussed.

Keywords Titanium alloy · Oxidation · Recrystallization · Gallium

Introduction

The reduction of weight and enhancement of gas-turbine working temperature are two important aspects of future aircraft engine development, as they could contribute to kerosene savings due to the improvement of jet-engine working efficiency [1, 2]. Near-α titanium alloys are attractive structural materials with a high strength-to-density ratio and excellent corrosion resistance, and they have been applied to jet-engine components operating at high temperature [3]. However, when exposed to gaseous environments containing oxygen, especially at elevated

✉ T. Kitashima
KITASHIMA.Tomonori@nims.go.jp

[1] Kyushu University, Fukuoka 810-0395, Japan

[2] National Institute for Materials Science, 1-2-1 Sengen, Tsukuba, Ibaraki 305-0047, Japan

temperatures, the mechanical properties of titanium-alloy components degrade, limiting the high-temperature capability during service and hindering commercial application. The interaction of titanium alloys with oxygen not only results in the oxygen embrittlement of the substrate zone of the components due to the high solubility of oxygen [4–7], but also causes a loss of ductile metallic material due to the formation of oxides on the surface [8, 9]. The oxidation behavior of titanium alloys is strongly affected by alloying additions, microstructure, and the oxidizing environment [10].

Many researchers have examined the influence of certain elements on the oxidation behavior of titanium-based alloys [8, 11–21]. Chaze et al. [11, 12, 14, 16] found that Al and Si caused a significant reduction in the amount of oxygen dissolved in the metallic phase during oxidation, whereas the effect of Cr was negligible. They also found that low amounts of Al and Si slightly decreased the adherence of the oxide layer to the metal substrate, while high amounts of Al and Si increased it; furthermore, Cr improved the adherence of the oxide layer. Johnson et al. [8, 13] and Chuanxi and Bingnan [15] found that the addition of Nb and W improved surface stability and suppressed oxide-scale formation, while the addition of V enhanced oxide-scale formation. Kitashima et al. [19–21] systematically investigated the oxidation behavior of near-α titanium alloys with the addition of a variety of elements and found that Sn and Ge segregate at the oxide/substrate interface, while Mo, Nb, W, Ga, Zr, and Hf dissolve in the internal TiO_2 scale without segregating at the TiO_2/substrate interface. The authors also demonstrated the role of each element by regression analysis and found a good correlation with alloy compositions, where the squared multiple correlation coefficient was 0.93 [21]. The oxidation behavior of α and α–β alloys is mainly dominated by the TiO_2 kinetics because the amount of Al is not sufficient to form a continuous Al_2O_3 layer [22].

There have also been reports on the effect of alloying elements on the formation of TiO_2 and Al_2O_3 in TiAl-based intermetallics. Shida and Anada [23, 24] investigated the effects of a variety of ternary elements on the oxidation behavior of a TiAl intermetallic compound and found that Cu, Y, V, Cr, and Mn enhanced the weight gain of alloys; Sn, Zr, Hf, Ta, Ni, and Co had little effect on the weight gain of alloys; and Si, Nb, Mo, and W reduced the weight gain of alloys, where W and Mo showed the highest reduction of weight gain. The authors also suggested that the enrichment of W and Mo in the metal side of the oxide/metal interface caused the formation of a Mo- or W-rich β-Ti and/or δ-Ti phase, which led to a more rapid supply of Al into the scale and/or formation of an Al_2O_3 layer along the interface. Yoshihara et al. [25, 26] systematically investigated the effects of Nb addition on the oxidation behavior of TiAl and found that Nb remarkably suppressed TiO_2 growth. Taniguchi and Shibata [27] found that a relatively low addition of Zr or Hf resulted in the formation of highly protective alumina scales. Some mechanisms have been previously discussed as follows: (1) The valence-control rule: Additional elements that can decrease the oxygen vacancies in TiO_2 effectively decrease the overall oxidation rate such as Nb [26]; (2) The formation of a barrier layer: A discrete layer aggregates in the scale near the oxide/substrate interface, working as a

barrier to some extent for Si [23]; (3) Wagner's scaling model: Internal oxidation changes to external oxidation to form a continuous alumina layer [28].

It should be noted that the oxidation behavior is also affected by the microstructure morphology [29–31]. Perez [29], Pitt and Ramulu [30], and Yang et al. [31] investigated the effects of grain size on the oxidation behavior of titanium alloys and pure titanium by both experiment and simulation and suggested that a higher grain size resulted in a lower weight gain of both titanium alloys and pure titanium during oxidation, mainly because of the lower grain boundary/grain ratio. Tiley et al. [32] demonstrated that the lath orientations in Ti-6242S affected oxygen diffusivity, in turn affecting the depth of oxygen ingress in this alloy. Leyens et al. [33, 34] investigated the effects of microstructures of IMI834 and TIMETAL1100 on the oxidation behavior and showed that, in both alloys, the fully lamellar structure gained less weight than the bimodal structure, which may mainly be due to the relatively lower grain boundary/grain ratio as explained by the authors. Zhang et al. [17] also reported similar results for the bimodal and fully lamellar microstructure, and the reason for phenomenon was suggested to be the fact that the primary α phase in the bimodal structure promoted the fast growth of TiO_2. However, there have been few reports on the combined effects of alloying elements and microstructure on the oxidation behavior of titanium alloys.

α-stabilizing elements, Al, Ga, and Sn, promote high-temperature strength in titanium alloys by solid solution strengthening [35]. In addition, the addition of these elements promotes the precipitation of the α_2 phase with the $D0_{19}$ structure, which results in dispersion strengthening and low ductility [35]. The Al equivalence, which is calculated as $Al + 1/2 \times Ga + 1/3 \times Sn + 1/6 \times Zr + 10 \times O$ in wt% [21], has been used to evaluate ductility after creep exposure. To avoid embrittlement, the Al equivalences of previous near-α titanium alloys have been set to be lower than 9. Sn, which is conventionally added in near-α titanium alloys, accelerates the oxide growth of TiO_2 and causes the spallation of oxides [19, 20, 36], while added Ga was found to dissolve in the oxide scale without segregation at the oxide/substrate interface in near-α titanium alloys [20]. Therefore, the replacement of Sn with Ga may be effective to design a new oxidation-resistant alloy. In this study, the oxidation behaviors of two near-α alloys containing Ga or Sn with the same Al equivalence were investigated, and the effect of microstructure in both alloys was examined.

Experimental Procedures

Near-α Ti alloy ingots TKT39 with added Sn and TKT41 with added Ga were produced by the cold crucible levitation melting method. The nominal chemical composition of the ingots is listed in Table 1. The Al equivalence values, calculated as $Al + 1/2 \times Ga + 1/3 \times Sn + 1/6 \times Zr + 10 \times O$ in wt% [21], were designed to be 9.5 for both TKT39 (Sn) and TKT41 (Ga). Each ingot was double-melted to enhance the compositional homogeneity. The cast ingots were β-forged at 1130 °C and then groove-rolled to 50% reduction at 980 °C in the α + β region to form square rods with sides of 14 mm. The β transus temperatures for TKT39 (Sn) and

Table 1 Chemical compositions (wt%), Al equivalence values, and β transus temperatures in TKT39 (Sn) and TKT41 (Ga)

Alloy	Ti	Al	Sn	≥Ga	Zr	Nb	Mo	Si	O	Al Eq.	T_β/°C
TKT39	80.3	7	4.5	–	6	1	1	0.2	0.053	10.0	985 ± 5
TKT41	81.8	7	–	3	6	1	1	0.2	0.093	10.4	995 ± 5

TKT41 (Ga) were 985 ± 5 and 995 ± 5 °C, respectively, as determined through microstructure observations after heat treatment at different temperatures. To obtain two different microstructures for each alloy, TKT39 (Sn) was heat-treated at two different temperatures, 965 °C (bimodal) or 1005 °C (fully lamellar), for 1 h, followed by air cooling, and TKT41 (Ga) was heat-treated at 970 °C (bimodal) or 1010 °C (fully lamellar) for 1 h, followed by air cooling. Subsequently, both alloys were aged at 700 °C for 2 h and air-cooled.

Cylindrical samples for oxidation tests were cut from the center of as-aged samples with a diameter of 8 mm and a height of 4 mm by wire electrical discharge machining. The surfaces of the specimens were finally polished using #800 SiC papers, followed by ultrasonic cleaning in acetone. Isothermal oxidation tests were performed at 750 °C in laboratory air. Each sample was placed in an alumina crucible, and the weight change was measured together with the weight of the crucible; therefore, spalled oxides scattered in the crucible were considered in the weight measurement. The samples in alumina crucibles were removed from the furnace after 20, 45, 70, 90, 110, 140, 240, 340, and 500 h of exposure. The mass change of each sample was measured using a microbalance with an accuracy of ±0.0001 g.

Microstructural characterizations of aged samples were performed using field-emission-gun scanning electron microscopy (SEM, ZEISS Auriga) at accelerating voltages of 5 and 15 kV. Samples for SEM observation were embedded in resin and polished using polishing papers and SiO_2. The volume fraction of the primary α phase was determined using the software ImageJ.

After the oxidation test, the constituent oxide phases were identified by X-ray diffraction (XRD) on a RINT2500 X-ray diffractometer using Cu Kα radiation, operated at 50 kV and 300 mA. Before microstructural characterization, the oxidized samples were cold mounted, cut, and metallographically polished by polishing papers and SiO_2. The cross-sectional microstructures of the oxidized samples were analyzed by SEM and electron backscatter diffraction (EBSD) attached to the SEM equipment at an accelerating voltage of 15 kV with the detector Ametek Digiview 5. Chemical analyses were performed using energy-dispersive X-ray spectroscopy (EDS) attached to the SEM equipment at an accelerating voltage of 15 kV with the detector Ametek Octane Super 60 mm^2.

Results and Discussion

The microstructure of as-heat-treated TKT39 (Sn) was bimodal with an equiaxed fine-grained primary α phase because the solution heat treatment at 965 °C is close to the β transus temperature (Fig. 1a). Solution heat treatment at 1005 °C, which is higher than the β transus temperature, produced a fully lamellar microstructure (Fig. 1b). The microstructure of TKT41 (Ga) was bimodal after solution heat treatment at 970 °C (Fig. 1c) and fully lamellar (Fig. 1d) after a solution heat treatment at 1010 °C. The volume fractions of the equiaxed α phase in bimodal TKT39 (Sn) and bimodal TKT41 (Ga) were 66.1 and 62.9%, respectively. The replacement of Sn with Ga increased the β transus temperature from 985 ± 5 to 995 ± 5 °C. Silicide precipitates can be observed as bright spots in Fig. 1a and c.

Figure 2 shows the weight gain of a sample per unit area for TKT39 (Sn) and TKT41 (Ga) alloys with bimodal and fully lamellar microstructures oxidized in laboratory air for up to 500 h at 750 °C. The overall weight gains of TKT39 (Sn)-bimodal, TKT39 (Sn)-lamellar, TKT41 (Ga)-bimodal, and TKT41 (Ga)-lamellar were 5.55, 4.78, 1.92, and 1.72 mg/cm^2, respectively, after oxidation for 500 h at 750 °C. The weight gain of TKT39 (Sn) was considerably greater than that of TKT41 (Ga) in both bimodal and fully lamellar microstructures, and the weight gain difference between these two alloys increased with the increase in exposure time.

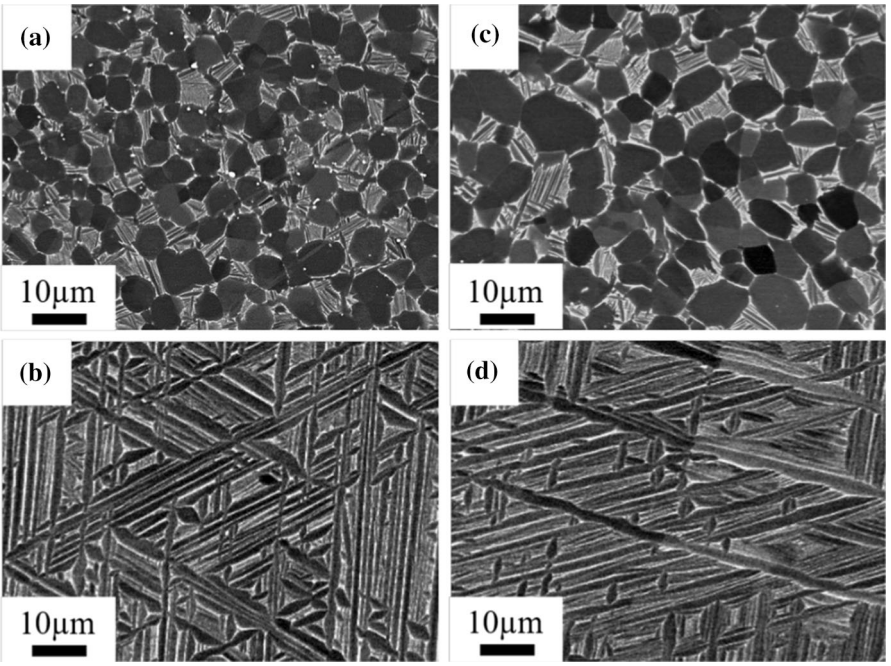

Fig. 1 Backscattered electron images of heat-treated alloys: **a** TKT39 (Sn)-bimodal, **b** TKT39 (Sn)-lamellar, **c** TKT41 (Ga)-bimodal, and **d** TKT41 (Ga)-lamellar

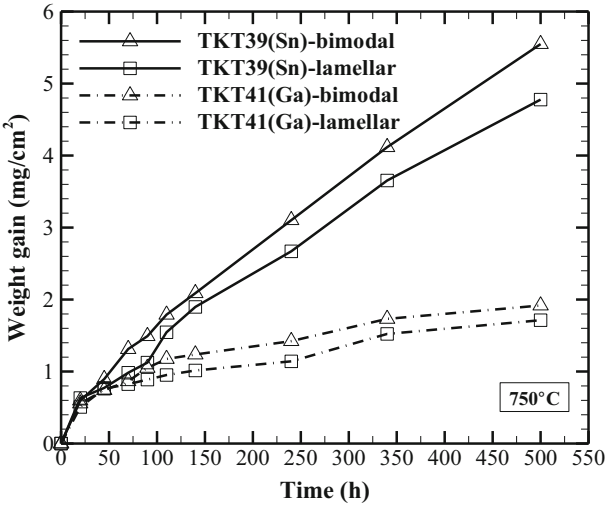

Fig. 2 Weight gains for specimens of TKT39 (Sn) and TKT41 (Ga) with bimodal and lamellar structures oxidized at 750 °C for up to 500 h

The weight gain during isothermal oxidation is due to oxide formation and oxygen dissolution, which depends on the alloy composition and microstructure [8, 34]. In both alloys, the bimodal structure gained more weight than the fully lamellar structure, which is consistent with previous studies [16, 33, 34]. In addition, the TKT41 (Ga) alloy with bimodal structure showed significantly lower weight gain (1.92 mg/cm^2) compared to the TKT39 (Sn) alloy (4.78 mg/cm^2) with fully lamellar microstructure, which indicated that Ga plays a more important role in oxidation behavior than microstructure in this study. The spallation of oxides on the surface of TKT39 (Sn) with both microstructures was observed after the oxidation test, as shown in Fig. 3a and b. The replacement of Sn with Ga clearly suppressed the spallation of oxides, as shown in Fig. 3c and d.

The surfaces of oxidized specimens were analyzed by XRD. Three different phases were distinguished after the oxidation of TKT39 (Sn), and four different phases were distinguished in TKT41 (Ga), as shown in Fig. 4. The main oxide phases were TiO_2 (rutile) and α-Al_2O_3 for both alloys. Reflections of α-Ti were also detected from the matrix material in both alloys, which indicated that the X-rays penetrated the oxide scales during measurement. $(Ga, Al)_2TiO_5$ was confirmed on the surfaces of Ga-added TKT41 alloy, as suggested in [20]. The intensity ratios of TiO_2/Al_2O_3 for TKT39 (Sn) were 1.97 and 1.53 with the bimodal and lamellar microstructure, respectively. For TKT41 (Ga), the intensity ratios were 0.73 and 0.34 with the bimodal and lamellar microstructure, respectively. These results indicated that the replacement of Sn with Ga suppressed TiO_2 (rutile) formation or promoted Al_2O_3 formation on the surface.

The distributions of elements within the oxide layer and substrate after the oxidation of both alloys with different microstructures were examined by EDS

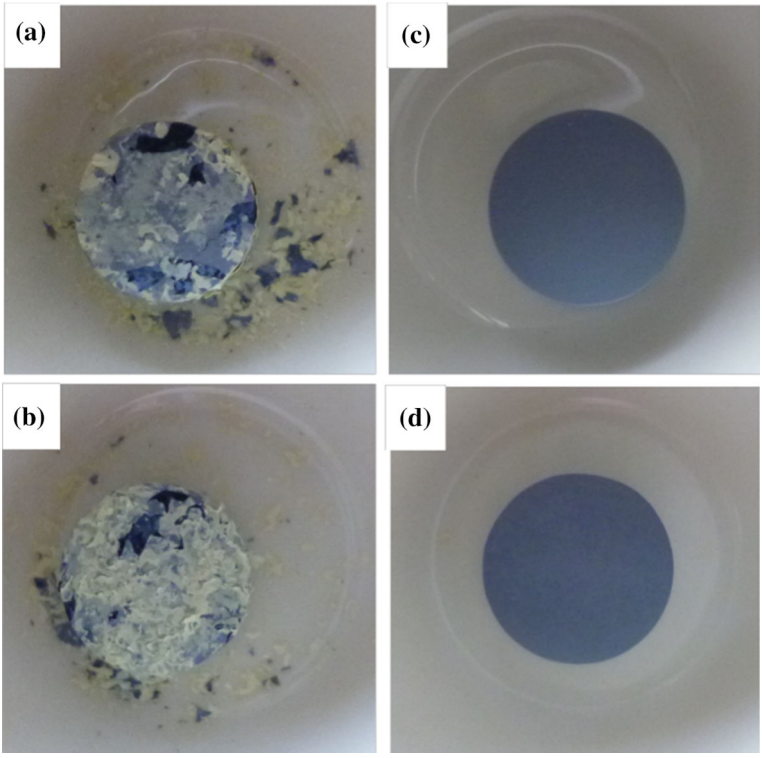

Fig. 3 Surfaces of **a** TKT39 (Sn)-bimodal, **b** TKT39 (Sn)-lamellar, **c** TKT41 (Ga)-bimodal and **d** TKT41 (Ga)-lamellar in crucibles after oxidation at 750 °C for 500 h

measurements. Figure 5 shows the concentration profiles of Al, Sn, Ga, Ti, and O in TKT39 (Sn) and TKT41 (Ga) along the red lines shown in backscattered electron (BSE) images. As shown in Fig. 5a and b, in the TKT39 (Sn) alloy, the thicknesses of the oxide scales were 14 and 11 μm for the bimodal and fully lamellar microstructure, respectively. Both oxides had a multilayer microstructure consisting of a heterogeneous mixture of TiO_2 and Al_2O_3. Sn was segregated in the substrate near the oxide/substrate interface in both TKT39 samples with different microstructures. In TKT41 (Ga), as shown in Fig. 5c and d, the thickness of the oxide scales consisting of external Al_2O_3 and internal TiO_2 was 2.7 and 2.5 μm for the bimodal and fully lamellar microstructure, respectively. The oxide layer in the Ga-added alloy was thinner owing to the suppression of oxide growth by the replacement of Sn with Ga. Unlike Sn, no segregation of Ga was observed at the oxide/substrate interface in TKT41 (Ga) for both microstructures. Ga was found to be enriched in the external Al_2O_3 layer in TKT41 (Ga) for both the bimodal and fully lamellar microstructures.

Oxide formation in Ti alloys has been well studied [18, 37], and an oxide multilayer consisting of TiO_2 and Al_2O_3 was formed in near-α Ti alloys. Similar multilayers consisting of several alternating TiO_2 and Al_2O_3 layers were observed in

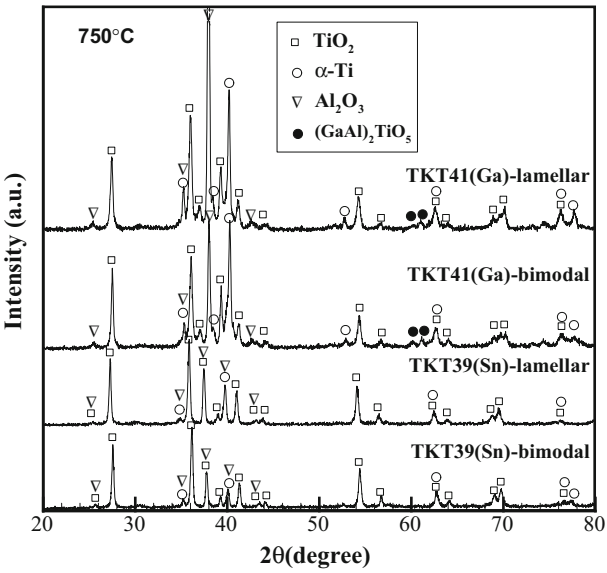

Fig. 4 XRD patterns of TKT39 (Sn)-bimodal, TKT39 (Sn)-lamellar, TKT41 (Ga)-bimodal and TKT41 (Ga)-lamellar oxidize at 750 °C

TKT39 alloy with added Sn, while in TKT41 alloy with added Ga, only a single outer Al_2O_3 layer and inner TiO_2 layer were observed. Similar results were obtained in [20]. Spallation occurred in Sn-added samples, and a clear segregation was observed at the oxide scale/substrate interface, while in Ga-added samples, no spallation nor segregation was observed. These results are consistent with previous studies [20]. Adherent oxides can provide acceptably low oxidation rates. In addition, the loss of the protective oxide by spallation will lead to high local oxidation rates of the alloy substrate [34]. (Ga, Al)$_2$TiO$_5$ [20] and a Ga-enriched layer corresponding to the Al-enriched layer near the oxide surface were detected in TKT41, and there was no evidence of the formation of nitrides, as described by Becker et al. [22, 33]. Kitashima et al. [20] demonstrated that (Ga, Al)$_2$TiO$_5$ may form near or in Al_2O_3 because gallium oxide may dissolve in Al_2O_3, which is based on the Ga_2O_3–Al_2O_3–TiO_2 phase system [38], and Ga addition may promote Al_2O_3 formation according to the decrease in the intensity ratios of TiO_2/Al_2O_3, which may act as a barrier that reduces the oxygen transfer flux, thereby decreasing the oxide growth rate [20].

Figure 6 shows the microstructure characteristics of TKT41 (Ga)-bimodal after oxidation for 500 h at 750 °C. In Fig. 6a, which shows the microstructure near the surface, a wavy layer was observed beneath the oxide layer. The compositions were determined by EDS, and the average Ga concentration in this wavy layer was approximately 5.23 wt%, which is greater than that in bulk (3.81 wt%). Such slight enrichment near the oxide can be also observed in Fig. 5c, which we will discuss later. Figure 6b and c shows EBSD results near the surface, including the oxide layer and the wavy layer beneath oxide layer in the substrate. As shown in the

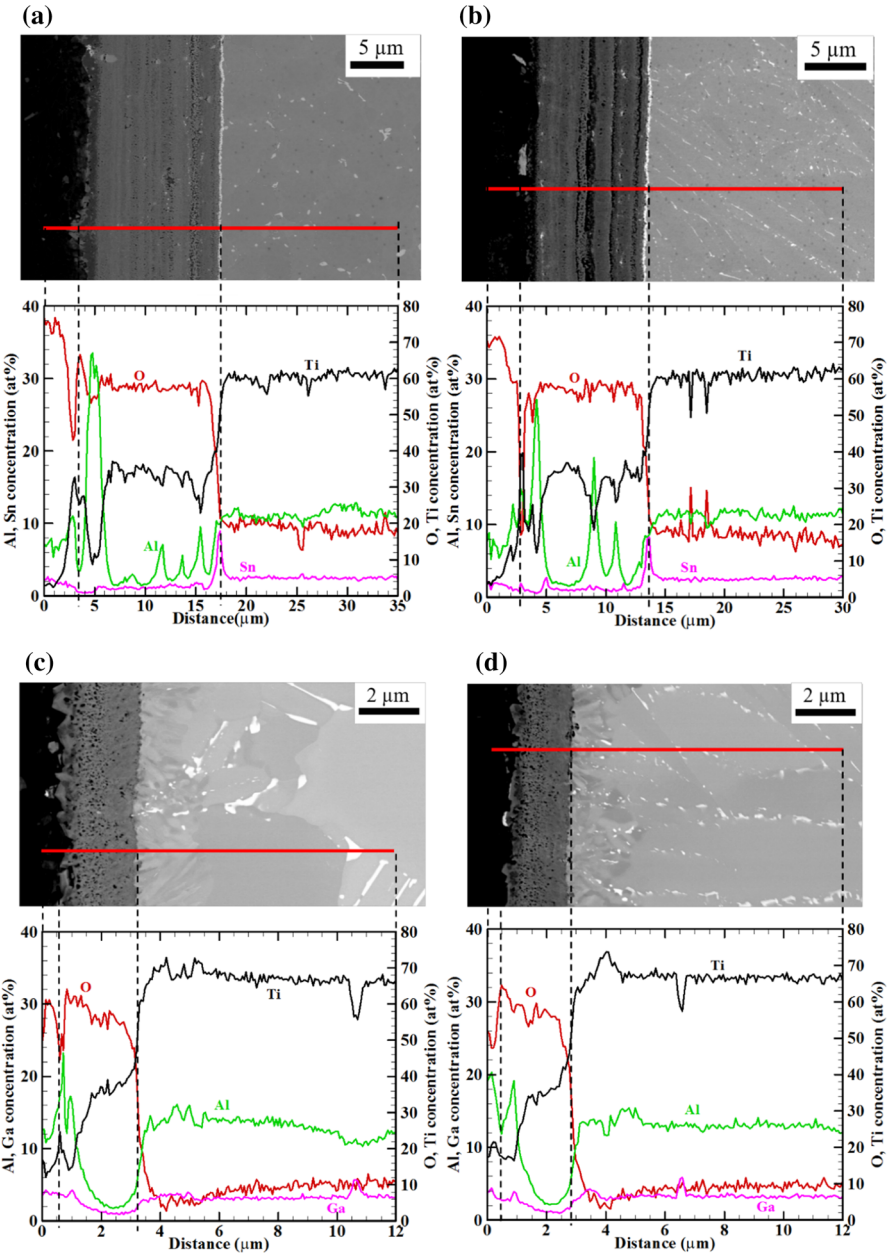

Fig. 5 Concentration profiles of Al, Sn, Ga, Ti and O obtained in the oxide and substrate along the lines for **a** TKT39 (Sn)-bimodal, **b** TKT39 (Sn)-lamellar, **c** TKT41 (Ga)-bimodal and **d** TKT41 (Ga)-lamellar after oxidation at 750 °C for 500 h

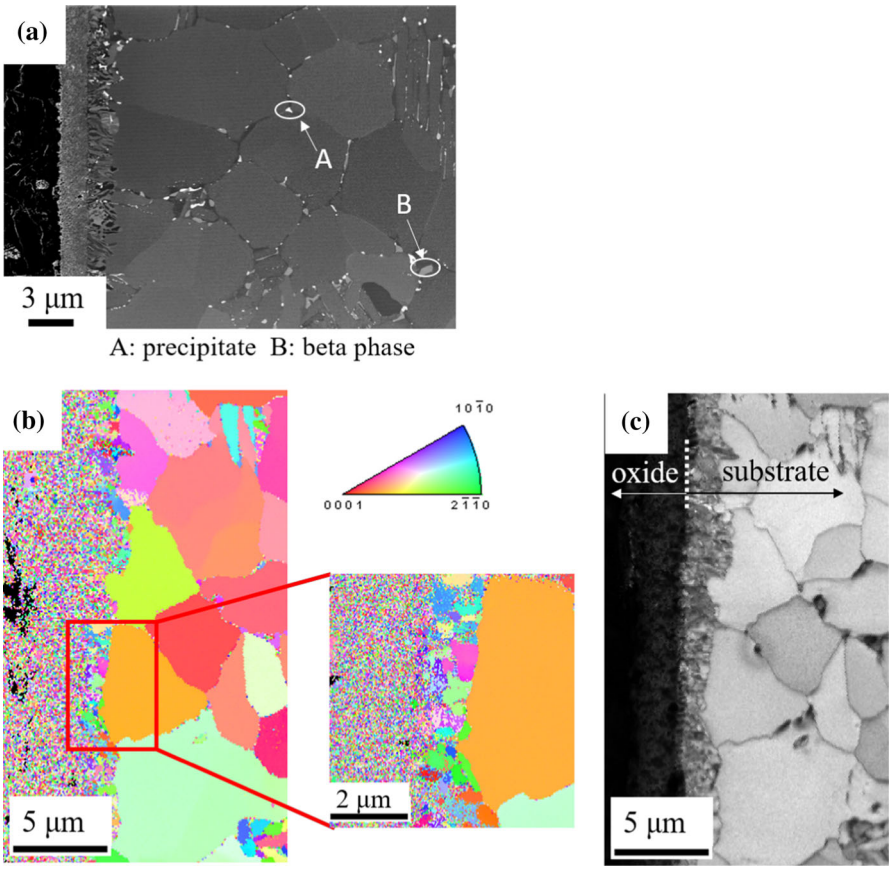

Fig. 6 Microstructure characteristics of TKT41 (Ga)-bimodal after oxidation for 500 h at 750 °C. **a** BSE image, **b** IPF map, and **c** IQ map near the surface

inverse pole figure (IPF) map of Fig. 6b, the wavy layer consisted of small grains with distinct orientation, and the grain size was approximately 0.5 μm, which is much less than substrate grain size of 5 μm. The image quality map (IQ map) EBSD data (Fig. 6c) also show distinct lines between the oxide layer and wavy layer as well as between the wavy layer and substrate. For comparison, the microstructure characteristics of TKT39-bimodal (Sn) after oxidation for 500 h at 750 °C are shown in Fig. 7. A clear boundary between the oxide layer and substrate was observed in both the IPF map (a) and IQ map (b). No small grains near the oxide scale were observed for TKT39 (Sn)-bimodal. The replacement of Sn with Ga promoted the formation of small grains.

There have been reports on recrystallization at the oxide/substrate interface during oxidation. In Ni–Cu alloy [39], the recrystallization may have occurred because of the diffusion of elements in the alloy, a phenomenon termed diffusion-

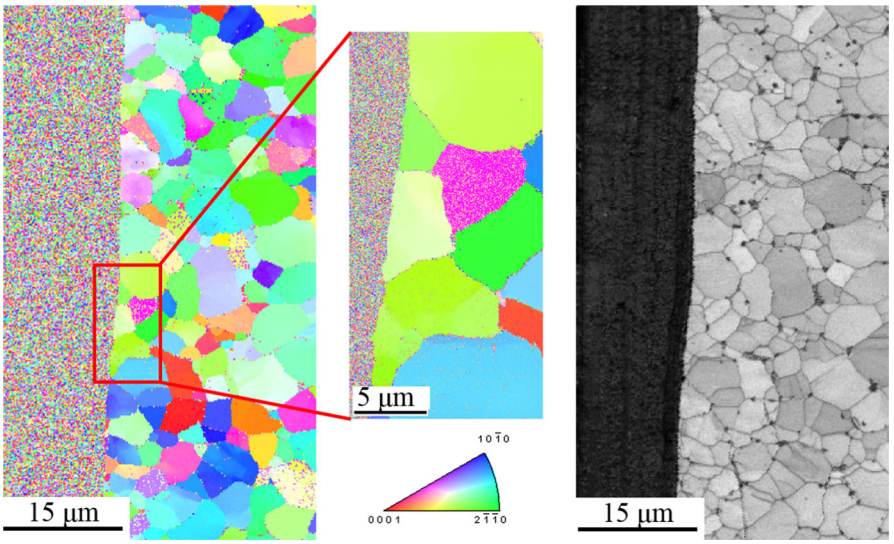

Fig. 7 Microstructure characteristics of TKT39 (Sn)-bimodal after oxidation for 500 h at 750 °C. IPF map (*left*) and IQ map (*right*)

induced recrystallization (DIR). A similar DIR phenomenon was observed in other systems such as Cu–Ni system [39], Ni–Fe system [40], alumina [41], and TiC [42]. However, to the authors' knowledge, the recrystallization process in Ti alloy has not yet been reported. To investigate the recrystallization process during oxidation, four TKT41 (Ga)-bimodal samples were prepared. Figure 8 shows the recrystallization process of TKT41 (Ga)-bimodal after exposure at 750 °C for (a) 20 h, (b) 45 h, (c) 90 h, and (d) 140 h, respectively. In Fig. 8a–d, the BSE image, EBSD IPF map, and EBSD IQ map are shown from left to right. As shown in Fig. 8a and b, at the beginning of the oxidation process, no distinct recrystallized grains were detected after exposure to air for 20 or 45 h at 750 °C. As the exposure time increased, the oxide layer as well as the recrystallized layer grew thicker and recrystallized grains grew larger; consequently, some small recrystallized grains with random orientations were observed, as shown in Fig. 8c and d.

Our results suggest that DIR may occur in the Ga-added Ti alloy during oxidation, as schematically shown in Fig. 9. We propose the following mechanism for the DIR. Initially, owing to the relatively higher activity of Ti compared to Al, TiO_2 is preferentially formed on the surface of Ti alloy [18]. Subsequently, Al^{3+} and Ga^{3+} cations diffuse outward through TiO_2 to form $(Al, Ga)_2O_3$ outside, and Ti^{4+} combines with the inward diffusion oxygen to form TiO_2 at the oxide/substrate interface. As the Ga^{3+} cation diffuses outward and Ga is enriched near the oxide/substrate interface, as shown in Fig. 5c, stress at the interface increased owing to plastic deformation with lattice distortion. This was suggested by TEM analysis in Cu–Zn alloy [43]. Subsequently, dislocation sub-boundaries are formed, resulting in the generation of recrystallized grains. Recrystallized grains grow larger with

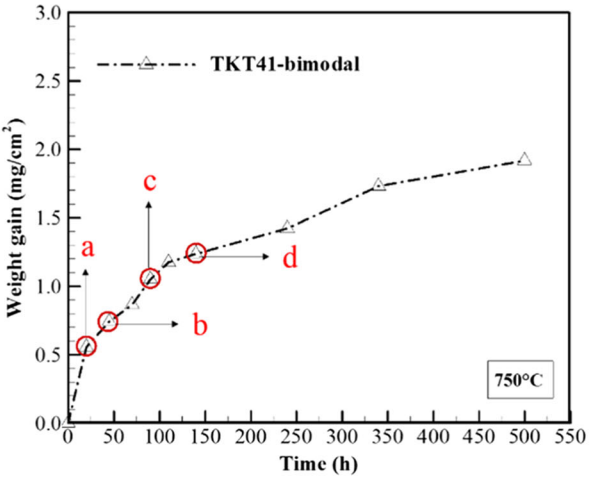
TKT41-bimodal
Weight gain (mg/cm²)
Time (h)
750°C
a
b
c
d

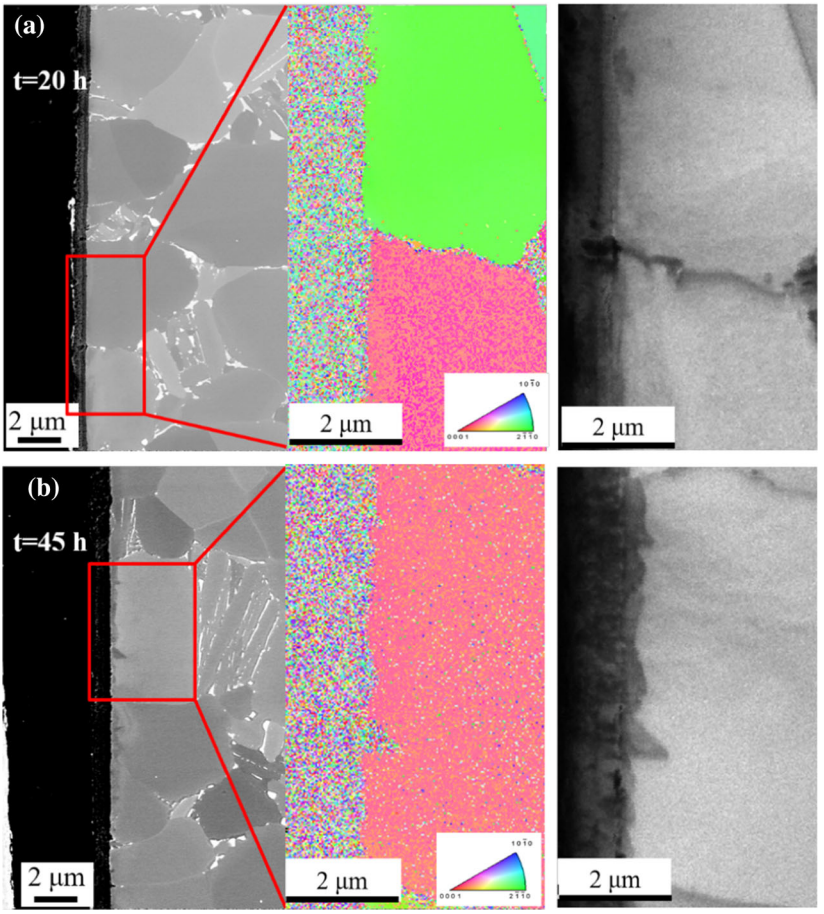
(a)
t=20 h
2 μm
2 μm
2 μm
(b)
t=45 h
2 μm
2 μm
2 μm

◀**Fig. 8** Recrystallization process of TKT41 (Ga)-bimodal after oxidation for **a** 20 h, **b** 45 h, **c** 90 h, and **d** 140 h at 750 °C. IPF map (*left*) and IQ map (*right*)

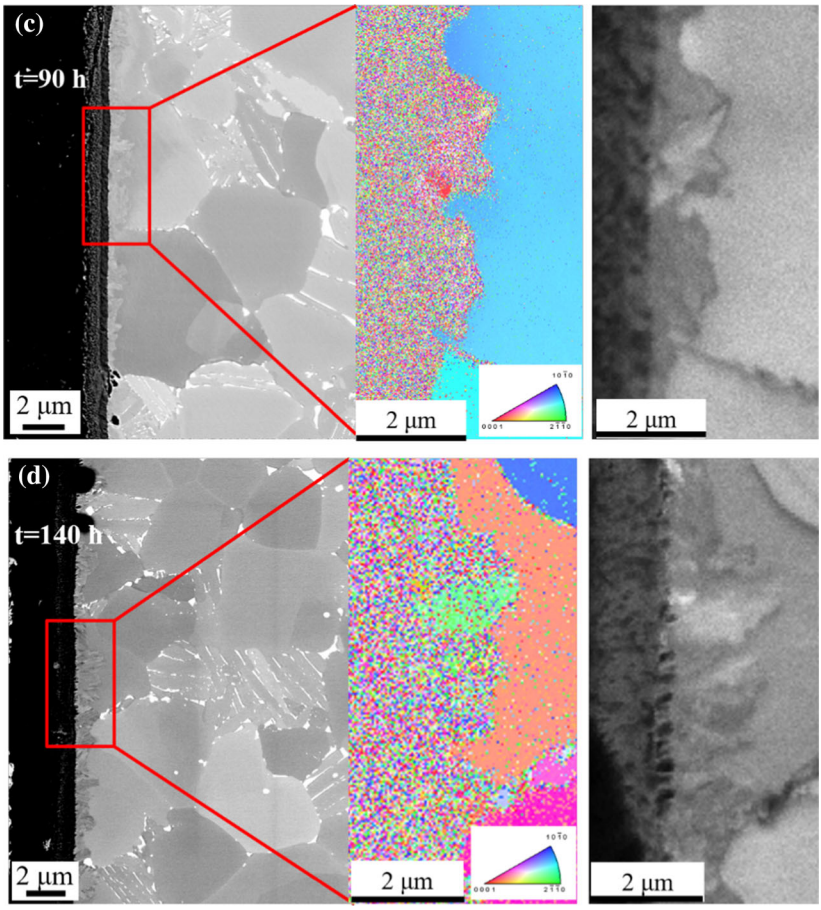

Fig. 8 continued

higher Ga concentration. This recrystallization process could release a part of the oxide/substrate interface stress, as suggested in Refs [44, 45], improving the adherence between the oxides and substrate and suppressing the oxide spallation in Ga-added Ti alloy. The temperature dependency of the recrystallization and the effect of the recrystallization on mechanical properties are the subjects of a future study.

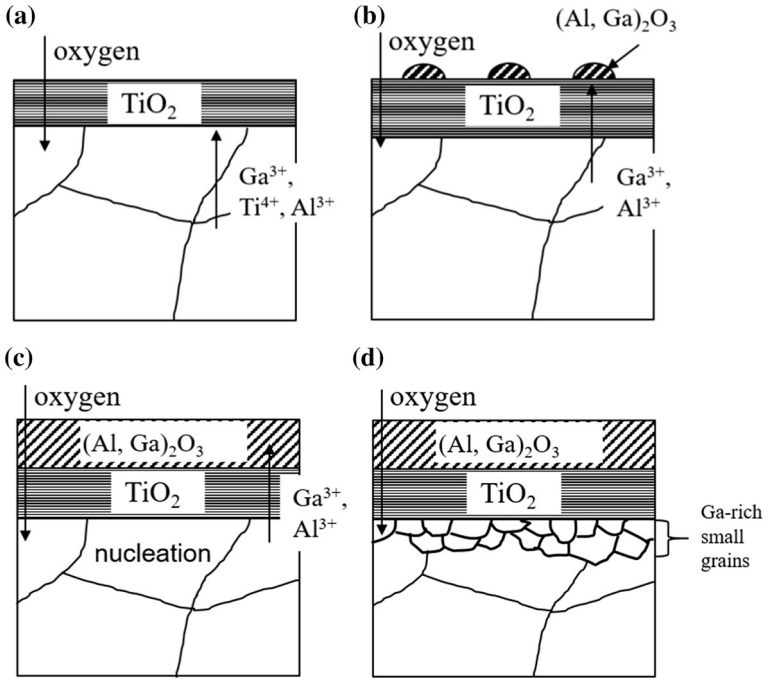

Fig. 9 Schematic representation of oxidation process of Ga-added Ti alloy. **a** Formation of TiO_2 layer, **b** Formation of $(Al, Ga)_2O_3$ layer, **c** Diffusion-induced recrystallization, **d** Recrystallized grains grow larger

Conclusions

The oxidation behaviors of two near-α titanium alloys containing Ga or Sn with bimodal structure and lamellar structure were investigated. Sn and Ga were set to have approximately equal Al equivalent values. The present study led to the following conclusions:

1. The replacement of Sn with Ga decreased the weight gain of the oxidation sample during oxidation, suppressed oxide growth, and improved adherence between the oxide and substrate. In Ga-added alloy, there was no Ga segregation at the oxide/substrate interface, and the formation of $(Al, Ga)_2O_3$ and $(Ga, Al)_2TiO_5$ was suggested.
2. The lamellar structure showed a smaller weight gain of the oxidation sample compared to the bimodal structure in both alloys. In addition, the Ga-added alloy with bimodal microstructure showed a smaller weight gain compared to the Sn-added alloy with lamellar structure.
3. In the Ga-added alloy, recrystallization occurred near the oxide/substrate interface, which may contribute to the release of stress, improvement of the adherence between the oxide and substrate, and prevention of the spallation of oxides.

Acknowledgements The authors gratefully acknowledge the support of the following staff members of the National Institute for Materials Science: Dr. Ayako Ikeda, Mr. Takaaki Hibaru, Mr. Shuji Kuroda, Mr. Kazuhiko Iida, and Mr. Koji Nakazato.

References

1. T. Kitashima, K. S. Suresh and Y. Yamabe-Mitarai, *Crystal Research and Technology* **50**, 2015 (28).
2. J. H. Perepezko, *Science* **326**, 2009 (1068).
3. G. Lütjering and J. C. Williams, *Titanium*, 2nd ed, (Springer, Berlin, 2003), p. 9.
4. R. N. Shenoy, J. Unnam and R. K. Clark, *Oxidation of Metals* **26**, 1986 (105).
5. Z. Liu and G. Welsch, *Metallurgical Transactions A* **19A**, 1988 (527).
6. T. Kitashima, L. J. Liu and H. Murakami, *Journal of the Electrochemical Society* **160**, 2013 (C441).
7. D. A. P. Reis, C. R. M. Silva, M. C. A. Nono, M. J. R. Barboza, F. Piorino Neto and E. A. C. Perez, *Materials Science and Engineering A* **399**, 2005 (276).
8. T. J. Johnson, M. H. Loretto, and M. W. Kearns, in *Proceedings of the Seventh World Titanium Conference* (Warrendale, PA, TMS), 2035 (1992).
9. K. S. Mcreynolds and S. Tamirisakandala, *Metallurgical and Materials Transactions A* **42A**, 2011 (1732).
10. C. Leyens and M. Peters, *Titanium and titanium alloys*, (Wiley-VCH, Weinheim, 2003), p. 213.
11. A. M. Chaze, G. Beranger and C. Coddet, *Titanium: Science and Technology*, (DGM, Oberursel, 1985), p. 2665.
12. A. M. Chaze and C. Coddet, *Journal of Materials Science* **22**, 1987 (1206).
13. T. J. Johnson, M. H. Loreto, C. M. Younes and M. W. Kearns, in *Second International Conference on the Microscopy of Oxidation* (Cambridge, London, England), 1 (1993).
14. A. M. Chaze and C. Coddet, *Oxidation of Metals* **28**, 1987 (61).
15. H. Chuanxi and L. Bingnan, in *Titanium'92: Science and Technology, Proceedings of the Seventh World Titanium Conference* (Warrendale, PA, TMS), 1891 (1992).
16. A. M. Chaze, C. Coddet, and G. Beranger, in *Sixth World Conference on Titanium*, (Part IV, Société Francaise de Métallurgic, France), 1765 (1988).
17. S. Z. Zhang, B. Zhou, N. Liu and L. Q. Chen, *Oxidation of Metals* **81**, 2014 (373).
18. H. L. Du, P. K. Datta, D. B. Lewis and J. S. Burnell-Gray, *Corrosion Science* **36**, 1994 (631).
19. T. Kitashima, Y. Yamabe-Mitarai, S. Iwasaki, and S. Kuroda, in *Proceedings of the 13th World Conference on Titanium* (Wiley, California, USA), 479 (2015).
20. T. Kitashima, Y. Yamabe-Mitarai, S. Iwasaki and S. Kuroda, *Metallurgical and Material Transactions A* **47A**, 2016 (6394).
21. T. Kitashima and T. Kawamura, *Scripta Materialia* **124**, 2016 (56).
22. S. Becker, A. Rahmel, M. Schorr and M. Schutze, *Oxidation of Metals* **38**, 1992 (425).
23. Y. Shida and H. Anada, *Corrosion Science* **35**, 1993 (945).
24. Y. Shida and H. Anada, *Materials Transactions* **34**, 1993 (236).
25. M. Yoshihara and Y. W. Kim, *Intermetallics* **13**, 2005 (952).
26. M. Yoshihara and K. Miura, *Intermetallics* **3**, 1995 (357).
27. S. Taniguchi and T. Shibata, *Intermetallics* **4**, 1996 (S85).
28. C. Z. Wagner, *Electrochemistry* **63**, 1959 (772).
29. P. Perez, *Corrosion Science* **44**, 2002 (1793).
30. F. Pitt and M. Ramulu, *Journal of Materials Engineering and Performance* **13**, 2004 (727).
31. Y. Yang, T. Kitashima, T. Hara, Y. Hara, Y. Yamabe-Mitarai, M. Hagiwara and L. J. Liu, *Materials Science Forum* **879**, 2016 (2187).
32. J. Tiley, J. Shaffer, A. Shiveley, A. Pilchak and A. Salem, *Metallurgical and Materials Transactions A* **45**, 2014 (1041).
33. C. Leyens, M. Peters and W. A. Kaysser, *Materials Science and Technology* **12**, 1996 (213).
34. C. Leyens, M. Peters, and W. A Kaysser, in the *Titanium'95: Science and Technology, Proceedings of the 8th World Conference on Titanium* (London: Institute of Materials, Birmingham, England), 1935 (1996).
35. C. E. Shamblen and T. K. Redden, *Metallurgical Transactions* **3**, 1972 (1299).
36. E. M. Kenina, I. I. Kornilov and V. V. Vanilova, *Metal Science and Heat Treatment* **14**, 1972 (396).
37. T. Kitashima and Y. Yamabe-Mitarai, *Metallurgical and Materials Transactions A* **46**, 2015 (2758).

38. A. L. Jaromin and D. D. Edwards, *Journal of American Ceramic Society* **88**, 2005 (2573).
39. D. Liu, W. A. Miller and K. T. Aust, *Metallurgical Transactions A* **19A**, 1988 (1667).
40. T. A. Parthasarathy and P. G. Shewmon, *Metallurgical Transactions A* **14A**, 1983 (2560).
41. Y. K. Paek, H. Y. Lee and S. J. L. Kang, *Journal of European Ceramic Society* **24**, 2004 (613).
42. K. W. Chae, C. S. Hwang, D. Y. Kim and S. J. Cho, *Acta Material* **44**, 1996 (1793).
43. S. S. Hackney, F. S. Biancaniello, D. N. Yoon and C. A. Handwerker, *Scripta Metallurgica* **20**, 1986 (937).
44. C. Coddet, A. M. Chaze and G. Beranger, *Journal of Materials Science* **22**, 1987 (2969).
45. J. Stringer, *Corrosion Science* **10**, 1970 (513).